A polarized cell system amenable to subcellular resolution imaging of influenza virus infection

Brault Jean-Baptiste, Thouvenot Catherine, Cannata Serio Magda, Paisant Sylvain, Fernandes Julien, Gény David, Danglot Lydia, Mallet Adeline, Naffakh Nadia

A polarized cell system amenable to subcellular resolution imaging of influenza virus infection

Brault Jean-Baptiste[1*], Thouvenot Catherine[2,3], Cannata Serio Magda[1#], Paisant Sylvain[1], Fernandes Julien[4], Gény David[5], Danglot Lydia[5, 6], Mallet Adeline[2,3], Naffakh Nadia[1*]

[1] Institut Pasteur, Université Paris Cité, CNRS UMR 3569, RNA Biology of Influenza Viruses, Paris, France

[2] Institut Pasteur, Université Paris Cité, Ultrastructural BioImaging Unit, 75015 Paris, France

[3] Institut Pasteur, Université Paris Cité, Photonic BioImaging Unit, 75015 Paris, France

[4] Institut Pasteur, Université Paris Cité, C2RT, Unit of Technology and Services Photonic BioImaging, F-75015 Paris, France

[5] Institute of Psychiatry and Neuroscience of Paris (IPNP), INSERM U1266, NeurImag facility, Université Paris Cité, 102 rue de la santé, 75014, Paris, France

[6] Institute of Psychiatry and Neuroscience of Paris (IPNP), INSERM U1266, Membrane Traffic in Healthy and Diseased Brain team, Université Paris Cité, 102 rue de la santé, 75014, Paris, France

current address: Institut Curie, PSL Research University, CNRS UMR144, Paris, France

* corresponding authors : jean-baptiste.brault@pasteur.fr, nadia.naffakh@pasteur.fr

Abstract

The life cycle of influenza A viruses (IAV), and notably intracellular trafficking of the viral genome, depend on multiple interactions with the cellular cytoskeleton and endomembrane system. A limitation of the conventional cellular models used for mechanistic study and subcellular imaging of IAV infection is that they are cultured in two dimensions (2D) under non-polarizing conditions, and therefore they do not recapitulate the intracellular organization of the polarized respiratory epithelial cells naturally targeted by IAVs. To overcome this limitation, we developed an IAV-infection assay in a 3D cell culture system which allows imaging along the baso-lateral axis of polarized cells, with subcellular resolution. Here we describe a protocol to grow polarized monolayers of Caco2-TC7 cells on static Cytodex-3 microcarrier beads, infect them with IAV, and subsequently perform immunostaining and confocal imaging, or electron microscopy, on polarized IAV-infected cells. This method can be extended to other pathogens that infect human polarized epithelial cells.

Introduction

Influenza viruses cause annual winter epidemics and are the leading cause of severe respiratory tract infections worldwide, with an estimated 500,000 deaths per year. Influenza A viruses (IAVs), which have an animal reservoir, can also cause pandemics with potentially devastating consequences in terms of mortality and economic loss [1]. Highly pathogenic avian IAVs of the H5N1 subtype, that are currently endemic in most parts of the world and have been found to infect and cause disease in many mammal species, are of great concern [2]. To support the much-needed development of advanced vaccines and anti-viral drugs, an improved understanding of the molecular mechanisms involved in the viral life cycle is required.

A limitation of most available data on influenza life cycle is that they derive from studies carried out in immortalized human cell lines cultured in two dimensions (2D) under non-polarizing conditions. These cellular models do not resemble the natural target tissue of IAVs, which is the polarized respiratory epithelium. Polarized and non-polarized epithelial cells exhibit a very different if not opposite organization of the cytoskeleton and molecular motors (kinesins versus dynein) used for anterograde and retrograde intracellular transport. Indeed, in non-polarized cells microtubules grow from a central centrosome towards the cell periphery, whereas in polarized epithelial cells the centrosome is apically-located and microtubules grow in the opposite direction, towards the centre of the cell (**Fig. 1A**, [3]). Consistently, post-Golgi secretion of anterograde cargoes was reported to be kinesin-driven in non-polarized HeLa cells [4] while it is regulated by dynein in polarized epithelial cells [5]. Therefore, cell polarization certainly has a strong impact on the cellular factors that contribute to the intracellular transport - including entry and exit - of viral components. Human primary nasal or tracheo-bronchial epithelial cells grown at the air–liquid interface (ALI) and differentiated into ciliated, secretory and basal cells, are being increasingly used to study the innate immune responses to infection or to screen antiviral molecules [6,7]. However, ALI cultures pose severe technical limitations for mechanistic investigations, in particular when subcellular imaging is required. Indeed, the polyester porous membrane on which the cells are grown generates high levels of light scattering, and the sample thickness (several tens of microns) induces chromatic aberrations which preclude confocal imaging along the baso-apical axis with a subcellular resolution. Sectioning of ALI samples is possible, however due to the stiffness of the polyester membrane it requires paraffin-embedding [8], which leads to significant fluorescent signal quenching and therefore restricts the possibilities of highly resolved imaging at the subcellular scale.

To provide a system of human polarized cells amenable to immunostaining and confocal imaging of IAV-infected cells with a subcellular resolution, we have adapted a 3D cell culture system on static microcarriers initially described by Jakob et al. for Madin-Darbin canine kidney (MDCK-II) cells [9]. We

first tested various human respiratory and/or epithelial cell lines known to support IAV growth (A549, Calu-3, NCI-H292, RPMI-1, 16HBE14, Caco-2/TC7), as well as quasi-primary, BMI-1-expressing bronchial epithelial cells derived from two distinct patients ([10], kindly provided by Ian Sayers, Nottingham University), for their ability to form monolayers of polarized cells on two types of micro-carrier : Cytodex 3, i.e. dextran beads coated with pig skin gelatin, or polystyrene beads (Corning). As assessed by the cell morphology, the only successful combination was Caco-2/TC7 cells grown on Cytodex 3 beads. Caco-2/TC7 is a subclone of the parental Caco-2 human colon epithelial cell line, with a highly efficient ability to polarize and differentiate [11]. We verified that the resulting polarized Caco-2/TC7 monolayer grown on Cytodex 3 beads can be efficiently infected by an IAV and support multicycle growth of infectious progeny virions, therefore it is suitable to study any phase of IAV life cycle.

As a proof of concept, we documented the late stages of the viral life cycle using confocal and electron microscopy. IAVs have a segmented, single-stranded RNA genome of negative polarity. Fully infectious virions contain eight viral RNA (vRNA) segments that range in length from 0.9 to 2.3 kb, and together encode ten major and several auxiliary proteins. Each vRNA is bound by several copies of the viral nucleoprotein (NP) and one copy of the viral polymerase, to form viral ribonucleoproteins or vRNPs. After viral entry by endocytosis, incoming vRNPs are imported into the nucleus where transcription and replication of the viral genome takes place. Newly synthesized vRNPs exit the nucleus and are transported to the sites of viral assembly and budding at the plasma membrane [12]. Although there is evidence that the cellular small GTPase RAB11A, the endoplasmic reticulum, and to some extent microtubules and actin filaments are involved (for review [13]), the precise underlying mechanisms of vRNP transport remain largely obscure. As the cytoskeleton and secretion pathway are involved, it is particularly relevant to investigate these late stages of IAV life cycle in a polarized cell system.

Caco-2/TC7 cells grown on Cytodex 3 beads were fixed in paraformaldehyde, co-stained with antibodies directed against RAB11A and the viral NP, the major component of vRNPs, and subsequently imaged using a Leica SP8 inverted confocal microscope equipped with 93x glycerol objective (NA=1.3, WD=300 µm) to provide an adequate depth of field and subcellular resolution. Alternatively, they were fixed in glutaraldehyde, processed for negative stain and resin-embedded for transmission electron microscopy. Optical slices or ultrathin sections going through the center of the Cytodex 3 beads were selected, as they displayed the baso-apical axis of the polarized epithelial cells. By using this protocol, we were able to visualize along the baso-apical axis the colocalization of vRNPs and RAB11A in cytoplasmic structures, the accumulation of vRNPs at the apical membrane, and the presence of viral-induced arrays of endoplasmic reticulum (ER) structures oriented parallel to the apical membrane.

Our protocol provides a reproducible, low-tech, low-cost and fast approach to perform subcellular imaging of IAV-infected polarized human epithelial cells along the baso-lateral axis, with standard confocal and electron microscopes. A limitation is that, in our hands, it could not be extended to other human epithelial cells beyond the Caco-2/TC7 cells, and these do not differentiate into a multi-cell type, mucus-secreting epithelium. However, compared to ALI cultures of human tracheo-bronchial cells, Caco-2/TC7 cells grown on Cytodex 3 beads present a number of advantages: in addition to being far more amenable to subcellular imaging, they provide a higher reproducibility, are easier to genetically engineer, require less expensive medium and consumables, and become polarized within two weeks instead of four to six weeks for ALI cultures. Importantly, Caco-2/TC7 cells grown on Cytodex 3 microcarrier beads recapitulate an essential feature of IAV natural tissue, which is polarity, and thereby allow to investigate the intracellular mechanisms of IAV replication in a context that is more relevant than non-polarized 2D cells cultures, notably regarding the trafficking of viral components in and out of the cell.

Materials and Methods

The protocol described in this manuscript is included for printing as **S1 Protocols**, and will be published on protocols.io upon acceptance.

Expected results

Four days after seeding Caco-2/TC7 cells on approximately 1500 Cytodex 3 beads (175 µm in diameter) with a ratio of approximately 600 cells per bead in a 35 mm dish, almost all beads are entirely covered with a confluent monolayer of cells. After filtering out of unattached cells and upon incubation of the beads for an additional period of 10-15 days, the cells acquire a columnar morphology (**Fig. 1B**). Immunostaining for Polarity protein Associated with LIN Seven-1 (PALS-1) and Zonula Occludens-1 (ZO-1) reveal the presence of an apical membrane domain (**Fig. 1 C**) and tight junctions (**Fig. 1D**), respectively, at the distal pole with respect to the bead surface, clearly indicating the formation of a polarized monolayer. Microvilli, tight junctions and an apically located Golgi apparatus can be visualized by transmission electron microscopy (**Fig. 1E**), further confirming that the Caco-2/TC7 cells are polarized after only 10-15 days of culture on Cytodex 3 beads.

Unlike in polarized cysts, the apical membrane of Caco-2/TC7 cells polarized on Cytodex 3 beads is oriented towards the medium, which facilitates infection assays. Indeed, upon infection with an IAV (A/WSN/33) at a high multiplicity of infection of 10 PFU/cell, around 70% of the cells from the Caco-

2/TC7 polarized monolayer are infected as assessed by immunostaining for the viral NP protein and confocal imaging of full beads (66.85% +/- 1.12% in three independent experiments, 2-5 beads examined in each experiment, approximately 80-100 cells per bead, 703 NP-positive cells out of 1053 in total) (**Fig. 2A**). Upon infection at a low multiplicity of infection of 0.01 PFU/cell, infectious viral particles accumulate in the supernatant to titers in the range of 10^5-10^6 PFU/mL. At 72 hpi, viral titers are at least 3-log lower in control beads treated with the specific IAV inhibitor baloxavir [14], which indicates that Caco-2/TC7 polarized monolayers support IAV multicycle growth and are therefore suitable to study any phase of IAV life cycle (**Fig. 2B**).

Upon confocal imaging of half beads with a 40x objective (NA=1.25, WD=350 µm) and by selecting optical slices sections that go through the center of the Cytodex 3 beads, the accumulation of viral vRNPs can be visualized at the apical membrane of polarized Caco-2/TC7 cells (**Fig. 3A,** upper panels, white arrowheads). In contrast, when non-polarized Caco-2/TC7 cells are infected and stained for NP at the same time-point, only few of them show vRNPs at the plasma membrane (**Fig. 3A,** lower panels, white arrowhead). At 8 hours post-infection (hpi), the percentage of infected cells displaying NP signal at the apical/plasma membrane was 13.3% in polarized and 2.5% in non-polarized cells, respectively (p-value=0.009) (**Fig. 3B**), suggesting that distinct transport pathways (dynein- versus kinesin-driven) may be taking place, which may impact kinetics of the viral cycle.

By using confocal microscopy with a 93x objective (NA=1.3, WD=300 µm), it is possible to reach subcellular resolution, and observe the accumulation of viral NP-positive punctate structures within the cytoplasm of infected cells (**Fig. 3C**, red colour), as well as their colocalization with the cellular RAB11A protein (**Fig. 3C**, cyan colour). These double-stained structures resemble those reported previously in non-polarized cell systems (e.g. [15,16]) and most likely represent an accumulation of vRNP transport vesicles. Interestingly, our imaging conditions reveal that at 8 hpi, the apical membrane is strongly positive for NP but not for RAB11A (**Fig. 3C** and a representative intensity plot in **Fig. 3D**), suggesting that vRNPs and RAB11A are dissociated before the vRNPs reach the apical membrane.

Finally, electron microscopy of polarized Caco-2/TC7 cells on beads enables to observe IAV-induced remodeling of the endomembrane system. The images shown in Fig. 4 were obtained after the beads were fixed in glutaraldehyde, processed for negative staining, dehydrated and resin-embedded for electron microscopy. Ultrathin sections going through the center of the beads were selected and observed using a transmission electron microscope at 120 kV. In mock-infected cells, the ER structures are sparse and of no particular orientation with respect to the apical membrane (**Fig. 4A**, left panel). In contrast, IAV-infected samples show arrays of elongated structures reminiscent of endoplasmic reticulum (ER) membranes oriented parallel to the apical membrane (**Fig. 4A**, right panel). Long (> 1 µm) ER structures are more frequent in IAV-infected cells (p-value < 0.001) (**Fig. 4B**). Interestingly, such

arrays of ER structures parallel to each other and to the plasma membrane were not observed in IAV-infected 2D cell cultures, which underscores the interest to use polarized cell models that better recapitulate the natural target tissue of the IAV, and more largely respiratory viruses.

Figures legends

Fig 1. Polarization of Caco-2/TC7 cells grown on Cytodex 3 microcarrier beads.

A. Schematic representation of the microtubule cytoskeleton organization in non-polarized versus polarized epithelial cells. In non-polarized cells the microtubules (in blue) grow from the centrosomes (pink cylinders) located near the nucleus and the Golgi apparatus towards the plasma membrane, whereas in polarized cells microtubules grow towards the basal pole. As a consequence, in non-polarized cells the molecular motors that move cargoes towards the plasma membrane are kinesins, the (+) end motors, whereas dynein, the (-) end motor, is moving cargoes towards the apical membrane in polarized cells.

B. Cellular morphology as observed with brightfield microscopy. A 10x objective was used (NA= 0.3, WD=550mm). A bead cross-section is shown in the inset to illustrate the columnar morphology of Caco-2/TC7 cells at 14 days post-seeding on the beads. Scale bars: 100 µm

C. Confocal imaging upon immunostaining for the PALS-1 apical membrane marker. A 40x objective (NA=1.25, WD=335µm) was used. Step size: 0.3 µm, pixel size: 0.4 µm, speed: 400 Hz. Scale bar: 25 µm

D. Confocal imaging upon immunostaining for the ZO-1 marker of tight junctions labelled with ATTO647n. A 93x Leica glycerol objective (NA=1.3, WD=300 µm) was used. Step size: 0.18 µm, pixel size: 61 nm, speed: 600 Hz. Scale bar: 10 µm

E. Electron microscopy of an ultrathin section. Caco-2/TC7 cells grown on Cytodex 3 beads were fixed with glutaraldehyde, post-fixed with osmium tetroxide, dehydrated and resin-embedded for transmission electron microscopy. A representative ultrathin section going through the center of the Cytodex 3 beads is shown. Endoplasmic and Golgi apparatus membranes, as well as a mitochondrion and a tight junction, are indicated by arrows. Scale bar: 1 µm

Fig 2. Influenza A virus infection of polarized Caco-2/TC7 cells.

A. 3D-reconstructed z-stack of half a Cytodex 3 microcarrier bead obtained by confocal imaging with a 40x objective (NA= 1.25, WD=335µm) upon immunostaining for the viral NP. Caco-2/TC7 cells grown on Cytodex 3 beads were infected at a MOI of 10 PFU/cell with the A/WSN/33 virus. At 8 hours post-infection (hpi) they were fixed with 4% paraformaldehyde and stained with a mix of antibodies specific for the viral NP or the cellular PALS-1 protein, and DAPI for nuclear staining. Blue, red and green colour: DAPI, NP and PALS-1 immunostaining, respectively. Step size: 0.3 µm, pixel size: 0.4 µm, speed: 400 Hz. Scale bar: 20 µm

B. Production of infectious IAV particles. Caco-2/TC7 cells grown on Cytodex 3 beads were infected at an estimated MOI of 0.001 PFU/cell with the A/WSN/33 virus, in the presence or absence of 0.1 µM of the viral inhibitor baloxavir. The supernatants were collected at 24, 48 and 72 hpi and titrated using a plaque assay. The data are represented as the mean +/- SD of four independent experiments. The dashed line represents the limit of detection (L.O.D.) of 250 PFU/mL.

Fig 3. Accumulation of influenza vRNPs at the apical membrane of polarized Caco-2/TC7 cells.

A. Caco-2/TC7 cells grown on Cytodex 3 beads (upper panels) or in standard 2D conditions (lower panels) were infected at an estimated MOI of 10 PFU/cell with the A/WSN/33 virus. At 8 hpi they were fixed with 4% paraformaldehyde, stained with an antibody specific for the viral NP (red colour) and with DAPI for nuclear staining (blue color), and imaged using a confocal microscope with a 40x objective (NA= 1.25, WD=335µm). Upper panels: an optical slice going through the center of a representative Cytodex 3 bead is shown. Step size: 0.3 µm, pixel size: 0.4 µm, speed: 400 Hz Scale bar: 25 µm. Inset scale bar: 10 µm. Lower panels: cells representative of the non-polarized state are shown. Step size: 0.3 µm, pixel size: 0.3 µm, speed: 400 Hz. Scale bar: 10 µm. White arrows indicate an accumulation of NP signal at the apical (upper panels) or plasma membrane (lower panels).

B. Percentage of cells showing NP signal accumulation at the plasma/apical membrane in non-polarized versus polarized Caco-2/TC7 cells, at 8 hpi with the A/WSN/33 virus at a MOI of 10 PFU/cell. Three independent experiments were performed, in total 634 non-polarized and 703 polarized cells were randomly selected and inspected visually for NP signal accumulation at the plasma/apical membrane, as indicated by white arrows in panel A. Significance was tested with an unpaired t test after log10 transformation of the data. ** p-value=0.009.

C. Caco-2/TC7 cells grown on Cytodex 3 beads were infected at an estimated MOI of 10 PFU/cell with the A/WSN/33 virus. At 8 hpi they were fixed with 4% paraformaldehyde, co-stained with antibodies specific for the viral NP (red colour) and the cellular RAB11A protein (cyan colour), and imaged using a confocal microscope with a glycerol 93x objective (NA=1.3, WD=300 µm). Step size: 0.18 µm, pixel size: 85.7 nm, speed: 600 Hz. Scale bar: 10µm. Inset scale bar: 5 µm. The yellow line corresponds to the intensity plot shown in panel D.

D. Fluorescence intensity profile for NP (red colour) and RAB11A (cyan) along the yellow line in drawn in Fig. 3C (overlay inset). The X axis indicates the distance in µM from the proximal (close to the cell center) extremity of the line.

Fig 4. Influenza virus-induced arrays of endoplasmic reticulum structures parallel to the apical membrane of polarized Caco-2/TC7 cells.

A. Caco-2/TC7 cells grown on Cytodex 3 beads were infected at a MOI of 10 PFU/cell with the A/WSN/33 virus or mock-infected. At 15 hpi they were fixed with glutaraldehyde, post-fixed with osmium tetroxide, dehydrated and resin-embedded for transmission electron microscopy. Representative ultrathin sections going through the center of the Cytodex 3 beads are shown. The lower panels represent a higher magnification of the region defined by the dotted line within the upper panels. Endoplasmic and Golgi apparatus membranes, as well as mitochondrion and tight junction, and, in the case of infected cells, extracellular virions, are indicated by arrows. Scale bar: 1µm, scale bar insets: 0.5 µm.

B-C. Distribution of the length of endoplasmic reticulum (ER) structures as observed in IAV-infected versus mock-infected cells. Images in the .ser format were opened using the TIA reader plugin of Image J to determine the pixel size. Plugin. Free-hand lines were drawn on apically located ER-like structures and their length was measured. Two independent experiments were performed. Five cells were used for each condition, 108 and 127 ER-like structures were measured for mock-treated and IAV-infected samples respectively. Significance was tested with an unpaired t test. *** p-value<0.001.

Supplementary information : S1 Protocols

Acknowledgements

We thank Véronique Carrière (Centre de Recherche Saint-Antoine, Paris, France) for providing the Caco-2/TC7 cells. We thank David Hardy and Marie Anne Rameix-Welti (Institut Pasteur, Paris, France), and Vincent Fraisier and Chloé Guedj (Institut Curie, Paris, France) for helpful discussions. This work was funded by a Human Frontiers Science Program (HFSP) grant held by NN (HFSP-RGP0040/2019), and a grant from the French National Research Agency (ANR) held jointly by NN and LD (FluNanotrack, ANR-21-CE11-0010-03). JBB was funded by the HFSP-RGP0040/2019 and the ANR-21-CE11-0010-03 grants. MCS was funded by the HFSP-RGP0040/2019 grant.

The UtechS Photonic BioImaging (Imagopole), C2RT, Institut Pasteur is supported by the French National Research Agency (France BioImaging, ANR-10-INSB-04-01, ANR-10–INBS-04 and ANR-10-LABX-62-IBEID).

The NeurImag Imaging core facility at the Institute of Psychiatry and Neuroscience of Paris is a member of the national infrastructure France-BioImaging supported by the ANR (ANR-10-INBS-04). We thank the staff of NeurImag imaging core facility for their scientific expertise in data acquisitions and the Leducq foundation or funding the Leica SP8 Confocal/STED 3DX system.

Competing interests

The authors declare no competing interests

References

1. Krammer F, Smith GJD, Fouchier RAM, Peiris M, Kedzierska K, Doherty PC, et al. Influenza. Nat Rev Dis Primers. 2018;4: 3. doi:10.1038/s41572-018-0002-y

2. Krammer F, Schultz-Cherry S. We need to keep an eye on avian influenza. Nat Rev Immunol. 2023;23: 267–268. doi:10.1038/s41577-023-00868-8

3. Fourriere L, Jimenez AJ, Perez F, Boncompain G. The role of microtubules in secretory protein transport. J Cell Sci. 2020;133: jcs237016. doi:10.1242/jcs.237016

4. Grigoriev I, Splinter D, Keijzer N, Wulf PS, Demmers J, Ohtsuka T, et al. Rab6 regulates transport and targeting of exocytotic carriers. Dev Cell. 2007;13: 305–314. doi:10.1016/j.devcel.2007.06.010

5. Brault J, Bardin S, Lampic M, Carpentieri JA, Coquand L, Penisson M, et al. RAB6 and dynein drive post-Golgi apical transport to prevent neuronal progenitor delamination. EMBO Reports. 2022 [cited 4 Oct 2022]. doi:10.15252/embr.202254605

6. Pizzorno A, Padey B, Dulière V, Mouton W, Oliva J, Laurent E, et al. Interactions Between Severe Acute Respiratory Syndrome Coronavirus 2 Replication and Major Respiratory Viruses in Human Nasal Epithelium. J Infect Dis. 2022;226: 2095–2104. doi:10.1093/infdis/jiac357

7. Zarkoob H, Allué-Guardia A, Chen Y-C, Garcia-Vilanova A, Jung O, Coon S, et al. Modeling SARS-CoV-2 and influenza infections and antiviral treatments in human lung epithelial tissue equivalents. Commun Biol. 2022;5: 810. doi:10.1038/s42003-022-03753-7

8. Zhanmu O, Zhao P, Yang Y, Yang X, Gong H, Li X. Maintenance of Fluorescence During Paraffin Embedding of Fluorescent Protein-Labeled Specimens. Front Neurosci. 2019;13: 752. doi:10.3389/fnins.2019.00752

9. Jakob PH, Kehrer J, Flood P, Wiegel C, Haselmann U, Meissner M, et al. A 3-D cell culture system to study epithelia functions using microcarriers. Cytotechnology. 2016;68: 1813–1825. doi:10.1007/s10616-015-9935-0

10. Torr E, Heath M, Mee M, Shaw D, Sharp TV, Sayers I. Expression of polycomb protein BMI-1 maintains the plasticity of basal bronchial epithelial cells. Physiol Rep. 2016;4: e12847. doi:10.14814/phy2.12847

11. Postal BG, Aguanno D, Thenet S, Carrière V. Rapid Evaluation of Intestinal Paracellular Permeability Using the Human Enterocytic-Like Caco-2/TC7 Cell Line. Methods Mol Biol. 2021;2367: 13–26. doi:10.1007/7651_2021_366

12. Hutchinson E, Fodor E. Transport of the Influenza Virus Genome from Nucleus to Nucleus. Viruses. 2013;5: 2424–2446. doi:10.3390/v5102424

13. Amorim MJ. A Comprehensive Review on the Interaction Between the Host GTPase Rab11 and Influenza A Virus. Front Cell Dev Biol. 2018;6: 176. doi:10.3389/fcell.2018.00176

14. O'Hanlon R, Shaw ML. Baloxavir marboxil: the new influenza drug on the market. Current Opinion in Virology. 2019;35: 14–18. doi:10.1016/j.coviro.2019.01.006

15. Amorim MJ, Bruce EA, Read EKC, Foeglein Á, Mahen R, Stuart AD, et al. A Rab11- and Microtubule-Dependent Mechanism for Cytoplasmic Transport of Influenza A Virus Viral RNA. J Virol. 2011;85: 4143–4156. doi:10.1128/JVI.02606-10

16. De Castro Martin IF, Fournier G, Sachse M, Pizarro-Cerda J, Risco C, Naffakh N. Influenza virus genome reaches the plasma membrane via a modified endoplasmic reticulum and Rab11-dependent vesicles. Nat Commun. 2017;8: 1396. doi:10.1038/s41467-017-01557-6

Figure 1

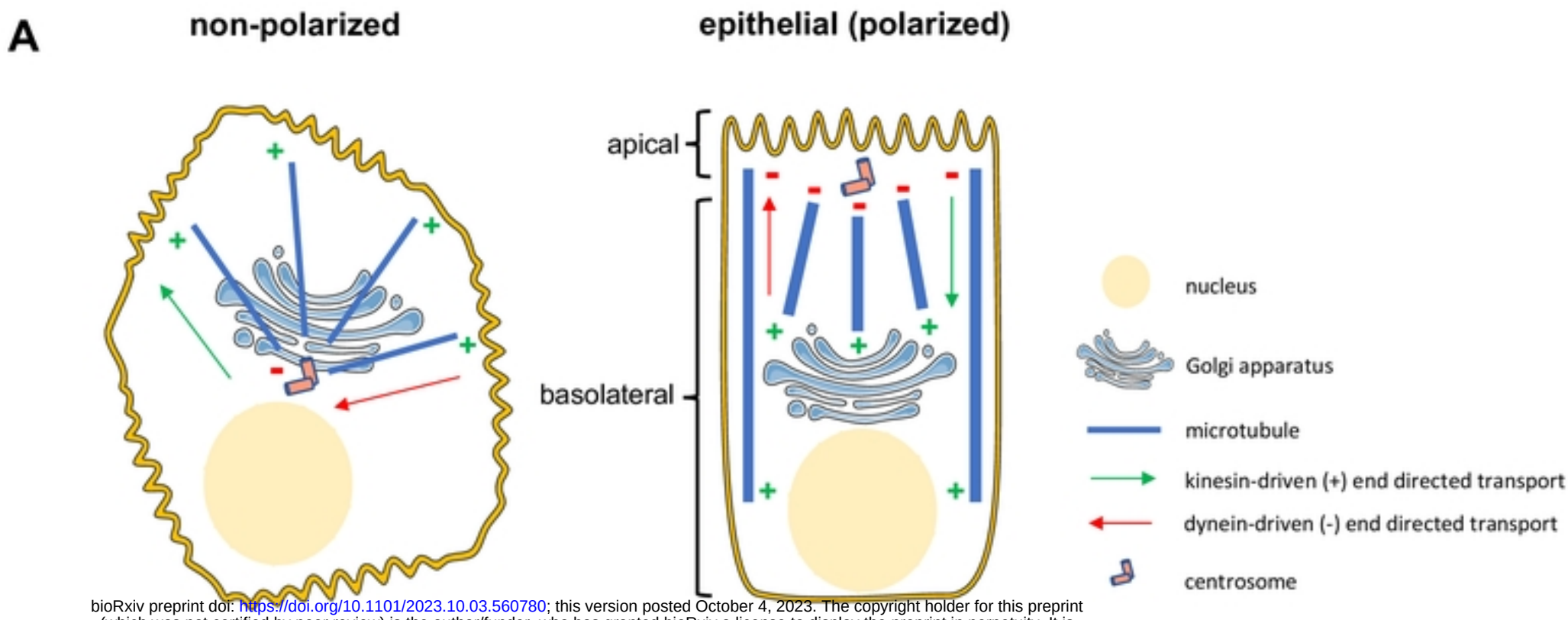

Figure 2

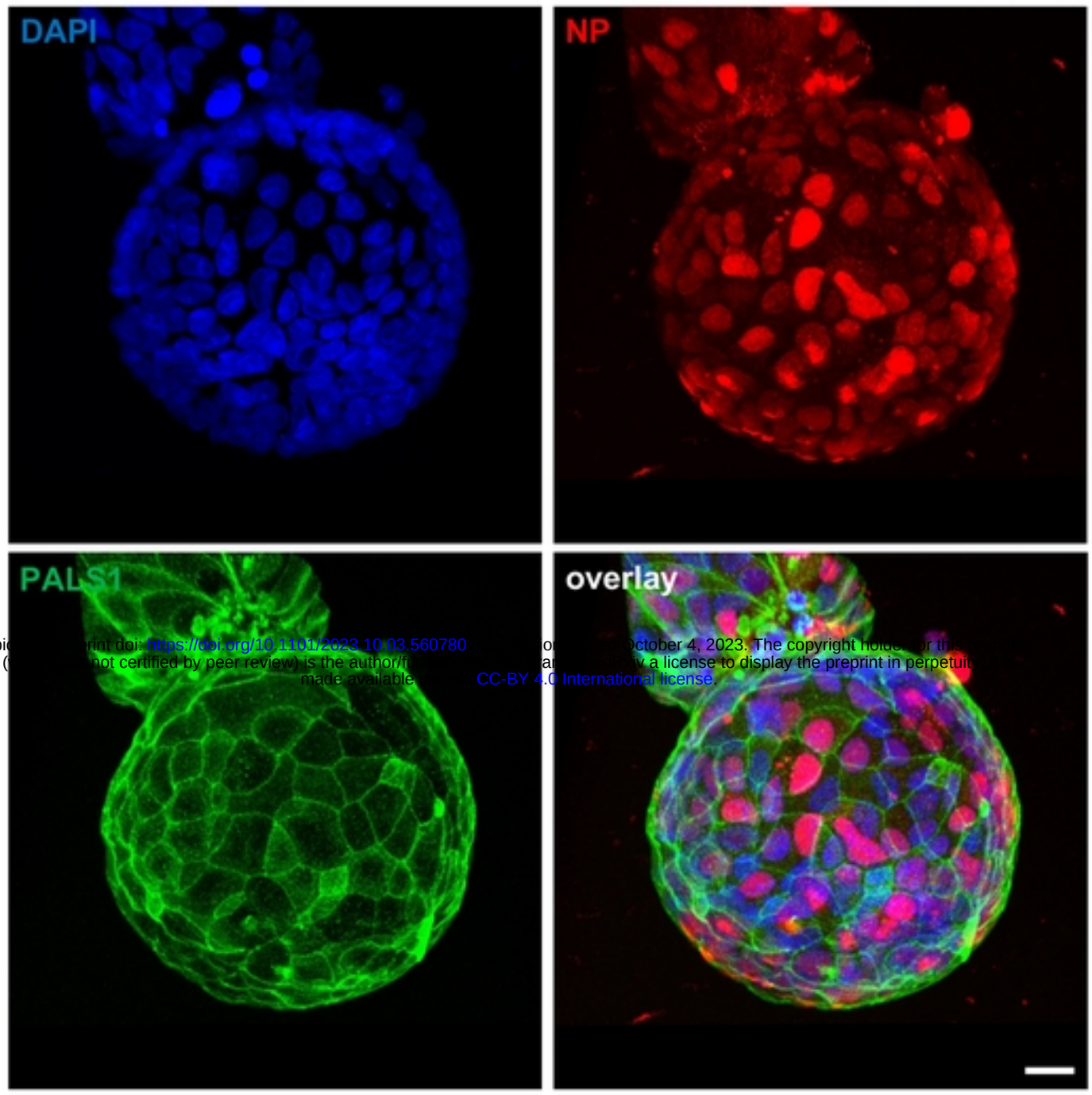

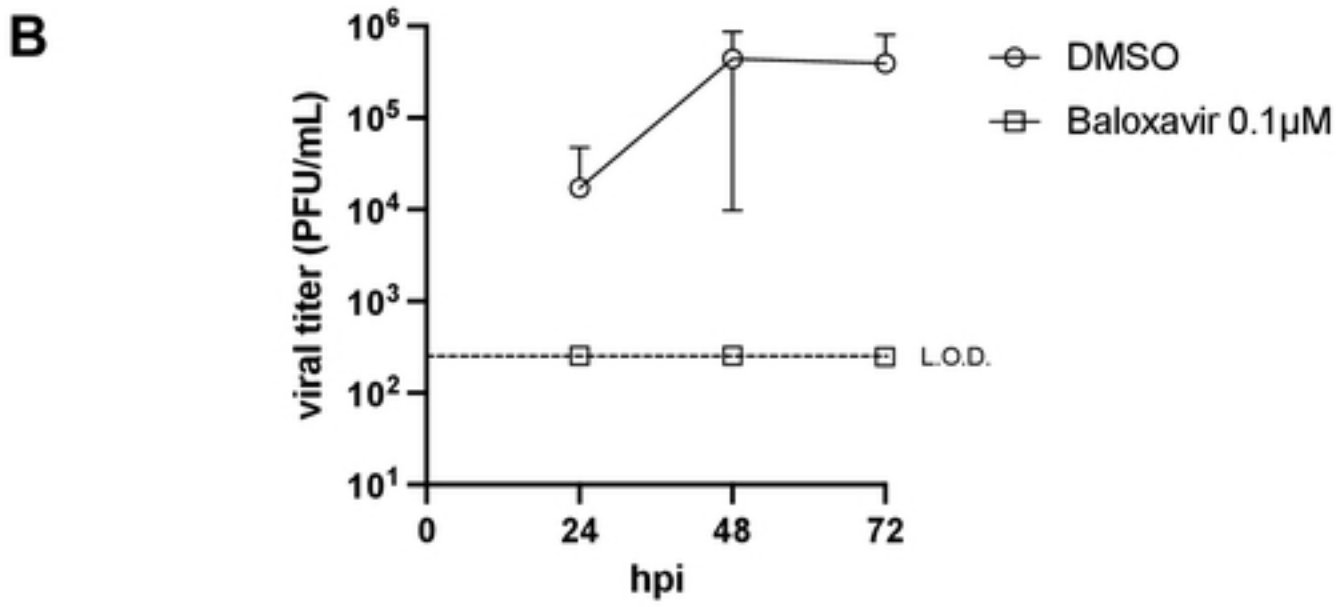

Figure 3

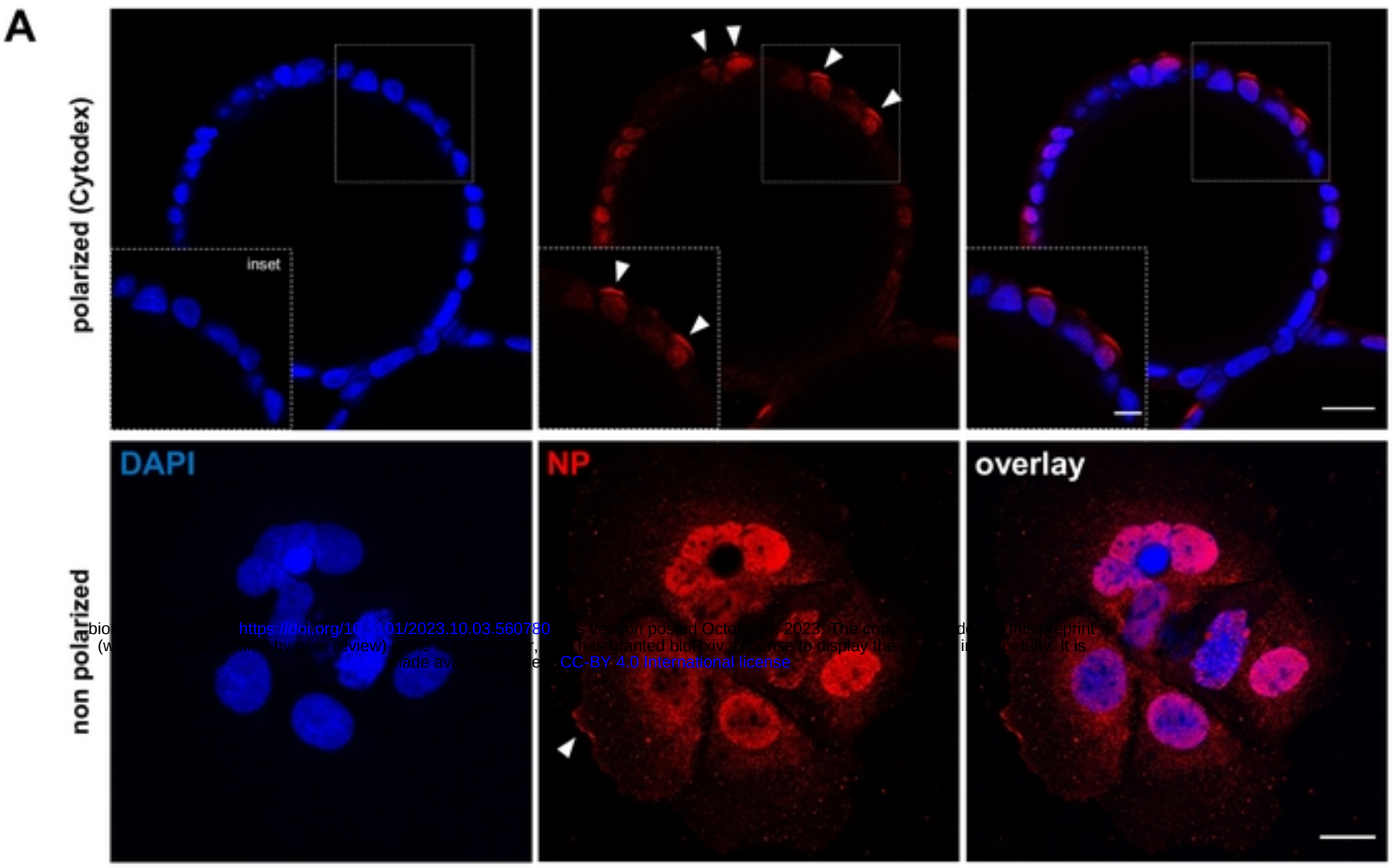

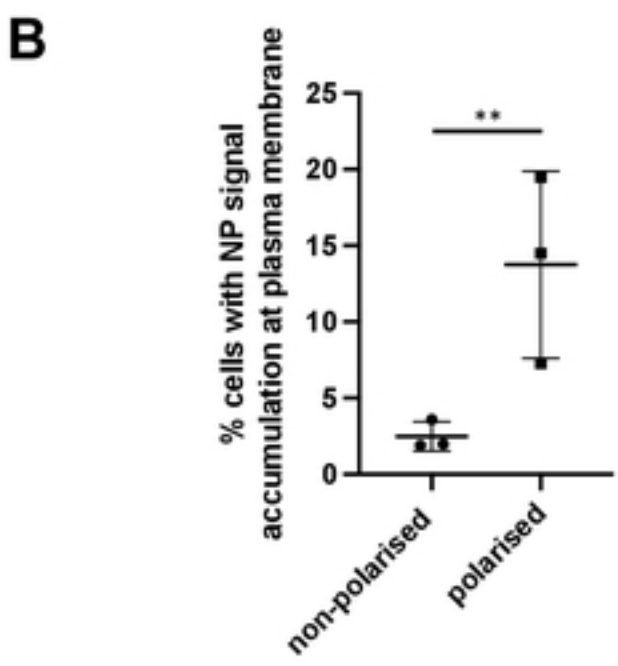

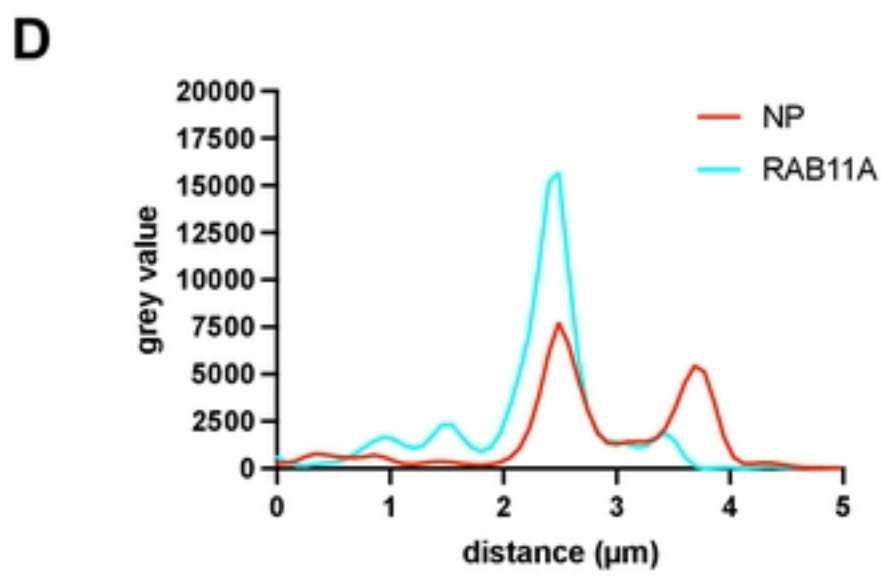

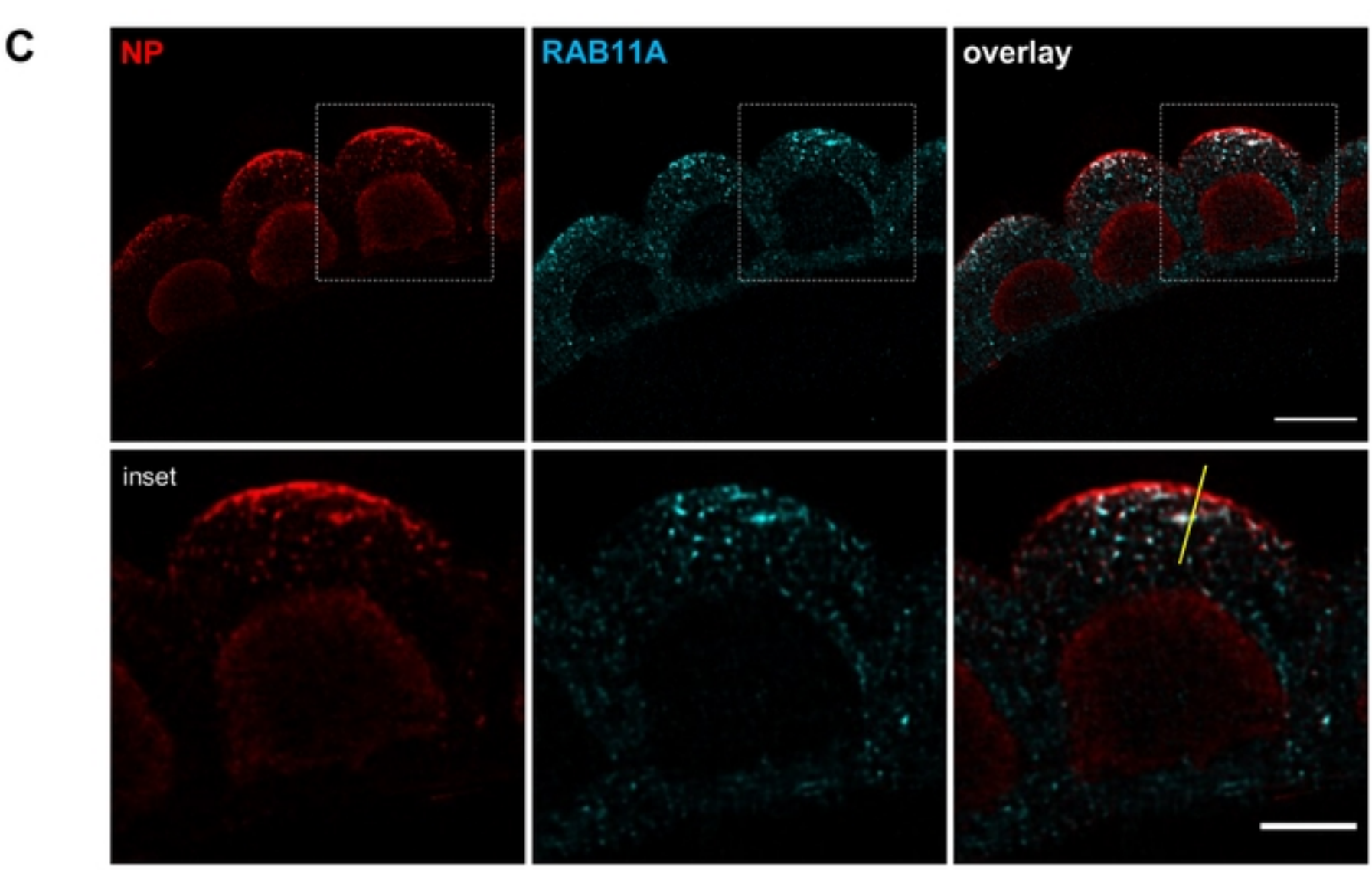

Figure 4